A Compact Low-Profile Differential Dual-Polarized Filtenna Without an External Filter Circuit for Vehicular Communications

Zhirui Zheng, Daotong Li, *Senior Member, IEEE,* Xiaoheng Tan, and Qiang Chen, *Senior Member, IEEE*

***Abstract*—A compact low-profile differential dual-polarized filtenna without an external filter circuit for vehicular communications is proposed in this paper. It has a compact, low-profile, simple, and symmetrical structure, which consists of four identical quarter circular patches with a pair of crossed feeding lines symmetrically and orthogonally embedded. Good filtering performance with three radiation nulls (RNs) generated without extra filtering structure is achieved, and the production mechanisms of three RNs are studied numerically. To get a deep insight into its working mechanism, the proposed structure is analyzed, and the equivalent lumped circuit is modeled and simulated. The prototype antenna with low profile of 2.832 mm and average gain of about 9.1 dBi within the frequency band of 5.28-6.11 GHz is fabricated and measured. Moreover, the measured polarization isolation is more than 44 dB within the operating band and the measured cross-polarization level is less than -29 dB. Good agreement between simulated and measured results can be acquired. The proposed antenna is a good candidate for in-vehicle local area networks (WLAN), in-vehicle Wi-Fi 6E, vehicle-to-vehicle (V2V) communication and 5G vehicle-to-basestation communication applications.**

***Index Terms*—Low profile, Differential, Dual-polarized, Filtenna**

I. Introduction

With the rapid development of vehicular technology and the demand for compact and low-profile components on vehicular platforms, much of radio frequency (RF) devices are integrated in the limited space of the vehicle As an indispensable RF front-end device, the antennas play a key role in vehicular communications. It is well known that dual-polarized antennas can reduce multipath effect suffered by vehicular communications, increase the channel capacity, and work duplex to reduce the volume of systems. Thus, the dual-polarized antennas with compact and low-profile configurations are desirable for vehicular communications and the limited vehicular space. However, due to increasingly scarcity of electromagnetic (EM) spectrum resources and the limited operating space of vehicle, the working bands of various devices are close, and the electromagnetic environment of the vehicle is complicated. As a result, conventional dual-polarized antennas are susceptible to out-of-band interference signals [1], and suffer coupling from other antennas or devices [2-3]. Moreover, integrating a large number of electronic devices in a limited space will lead to the serious electromagnetic compatibility (EMC) problems on vehicular platforms [4-9]. The EMC characteristics of the communication system will be destroyed greatly.

The dual-polarized filtennas has great application potential and prospect in suppressing out-of-band interferences, decoupling and achieving EMC [10-12]. Moreover, the volume of transceiver RF front-end can further be miniaturized, and the insertion loss introduced by the interconnection can be reduced greatly. Some design methods of dual-polarized filtennas have been reported [13-17]. However, in the dual-polarized filtenna design, generally, double-/multi-layer substrates [13-16] or relatively bulky extra filter circuit [17] is adopted, which is not easy to process and integrate, and leads to higher profile and more extra losses. As a result, although these designs own good filtering response, their incompact and high profile structure with additional filter circuits are not easy to be applied to vehicular platforms. Therefore, antennas with compact low-profile configurations and filtering response without an external filter circuit are highly desired for the dual-polarized filtenna design in vehicular communications.

As we all know, differential structures could improve common-mode suppressions [18-19] and reduce antennas' cross-polarization levels [20], which are of benefit to the EMC characteristics of communication systems on vehicular platforms. Differential-fed dual-polarized filtennas were proposed by utilizing eight short pins and slots etched on the ground and patch [21], and four C-shaped slots and four short pins [22], respectively. However, it lacks a radiation null (RN) in the lower stopband in [22], and has a narrow bandwidth with the fractional bandwidth (FBW) of only 1.69%. In [23], by using low temperature co-fired ceramic (LTCC) process (nine

This work was supported in part by the National Natural Science Foundation of China under Grant 61801059 and U20A200726, in part by the Basic Research and Frontier Exploration Special of Chongqing Natural Science Foundation under Grant cstc2019jcyj-msxmX0350, in part by the FY2021 JSPS Postdoctoral Fellowship for Research in Japan under Grant P21053, and in part by the Grant-in-Aid for JSPS Research Fellow under Grant 21F21053. *(Corresponding Author: Xiaoheng Tan.)*

Zhirui Zheng, Daotong Li and Xiaoheng Tan are with School of Microelectronics and Communication Engineering, Chongqing University, Chongqing 400044, China (e-mail: zhengzhirui666@163.com; dli@cqu.edu.cn; txh@cqu.edu.cn).

Daotong Li and Qiang Chen are with the Department of Communications Engineering, Tohoku University, Sendai 980-8579, Japan (qiang.chen.a5@tohoku.ac.jp).

layers) and loading an additional square ring and four differential L-type probes connected with open strips, a broadband dual-polarized differential filtenna with four RNs was realized. However, the complexity of processing and antenna cost are increased. Through loading the extra filtering circuit and four slots etched on the patch [24], a differential dual-polarized filtenna was obtained. Nevertheless, the complex and large overall configuration and the high profile of 11.3 mm are achieved because of the bulky differential dual-polarized filtering network. Furthermore, in [25], a compact dual-polarized filtenna with sharp roll-off rate was proposed, which two RNs were generated by stacked patches. However, due to four-layer substrates and thick air layers, the high profile of 20.03 mm is also inevitable. Thus, for vehicular communication applications, designing the differential dual-polarized filtennas with high performance and compact, low-profile and simple configuration is still quite challenging.

In this paper, a compact low-profile differential dual-polarized filtenna without an external filter circuit for vehicular communications is proposed. The main contributions of this paper are as follows: Firstly, by symmetrically and orthogonally embedding a pair of crossed feeding lines into four identical quarter circular patches printed on one substrate, it naturally meets the requirement of dual-polarization, differential feeding and coplanar waveguide structure, realizing the compact, low-profile, simple and symmetrical configuration, which is facilitates the integration in the limited space of the vehicle. Secondly, without utilizing slots, short pins, parasitic/stacked elements, L-shaped probes, open stubs and extra filtering circuits, using only the feeding line and quarter circular patches, filtering response and three deep RNs are generated through the self-structure of the proposed antenna, where one RN is generated by energy reflection and two RNs are introduced by far field electric field cancellation, avoiding the bulky differential dual-polarized filtering network and keeping the compact, low-profile and simple configuration. Additionally, the proposed antenna is tested to validation, showing high gain of 9.58 dBi, FBW of 14.6%, polarization isolation more than 44 dB, deep rejection level of 25 dB, low cross-polarization level less than -29 dB, three RNs and low-profile of 2.832 mm. The developed antenna is a good candidate for in-vehicle local area networks (WLAN), in-vehicle Wi-Fi 6E, vehicle-to-vehicle (V2V) communication and 5G vehicle-to-basestation communication applications.

II. Antenna Configuration and Analysis

The proposed low-profile dual-polarized filtenna with high gain and high polarization isolation is realized using differential feeding structures and only one substrate, and no external filter circuits are utilized. The proposed structure, and its electromagnetic characteristics simulated using High Frequency Structure Simulator 15.0 version (HFSS 15.0), are detailed as follows.

A. Antenna Configuration

The configuration of the proposed differential dual-polarized filtenna is illustrated in Fig. 1. It mainly consists of a pair of crossed feeding lines and four identical quarter circular patches, and all of them are printed on the top layer of the substrate Rogers 4350 with relative permittivity of 3.48, loss tangent of 0.004 and thickness h_1 of 1.524 mm. The crossed feeding lines with width of W_1 are placed orthogonally and symmetrically to meet differential input and dual-polarization. Each feeding line is directly fed by a couple of Sub-miniature version A (SMA) connectors with differential signals. Two T-Shaped branches with widths of W_2 and W_3 are loaded at both ends of each feeding line to adjust the antenna impedance. Besides, to avoid two feeding lines crossing each other, the middle part with width of W_6 of the feeding line in x direction is printed under the substrate, and connects with other sections on the top layer of substrate through two metal via holes. Moreover, four identical quarter circular patches with radius R are placed rotationally and symmetrically in the four quadrants formed by the two feeding lines. In addition, there is a very thin air layer with thickness h_2 of 0.8 mm between the substrate and the metal ground to achieve better impedance matching.

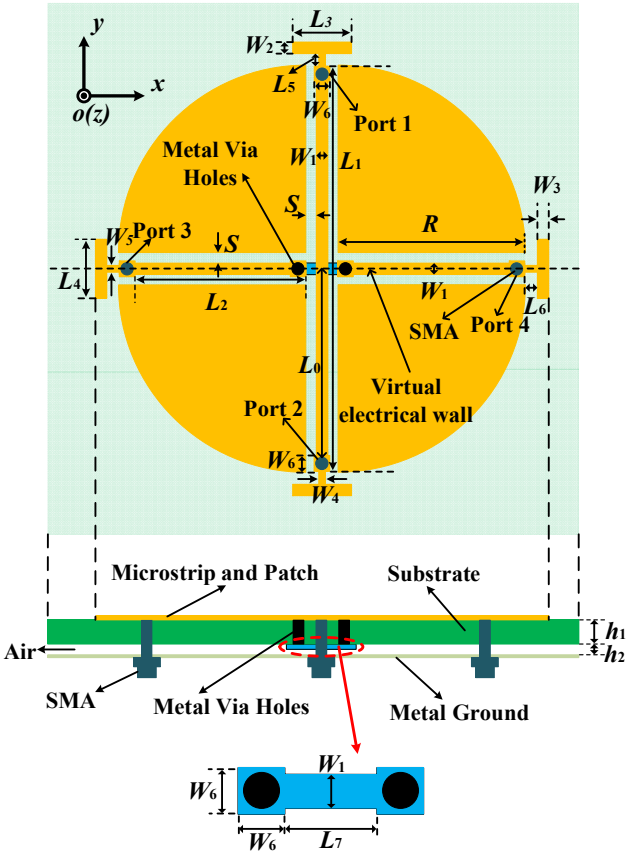

Fig.1. Configuration of the proposed antenna. (L_0=16.6, L_1=35.9, L_2=15.5, L_3=6.15, L_4=6.15, L_5=1.78, L_6=1.78, L_7=2.1, W_1=1.3, W_2=1.2, W_3=1.2, W_4=1, W_5=1, W_6=1.3, S=0.7, R=15. h_1=1.524, h_2=0.8, Unit: mm.)

B. Antenna Working Mechanism

Due to the symmetry of the proposed structure, both polarizations (vertical and horizontal polarization are in y and x direction, respectively) have the same working mechanism. Herein, only the investigations of vertical polarization are presented as example. In order to get a deep insight into the

antenna operating mechanism, five types of antennas named as ANT_I - ANT_V and the proposed filtenna are involved.

Case 1: Fig. 2(a) and (b) show the structures of ANT_I and ANT_II and their surface current distributions at f_1, respectively, and Fig. 2(c) displays their realized gains. It can be seen that there is no RN. Nevertheless, an obvious filtering roll-off property in the low frequencies is revealed, due to the weak coupling between the feeding line and the patch [26]. Furthermore, in Fig. 2(c), the first three resonance modes, i.e., $TM_{1/2,1/2}$, $TM_{1,1/2}$ and $TM_{1,1}$ modes, can be observed through $|S_{dd11}|$ curves. The corresponding vector electric field (v-E-field) distributions at the three modes are given in Fig. 3(a)-(f). Note that the single quarter circular patch exhibits the normal broadside radiation pattern at $TM_{1/2,1/2}$ and $TM_{1,1/2}$ modes, but the distorted radiation pattern at $TM_{1,1}$ mode, as shown in Fig. 3(a)-(c). Hence, $TM_{1,1}$ mode should be shifted to high frequency or suppressed. It can be concluded that each quarter circular patch operates normally at $TM_{1/2,1/2}$ and $TM_{1,1/2}$ modes.

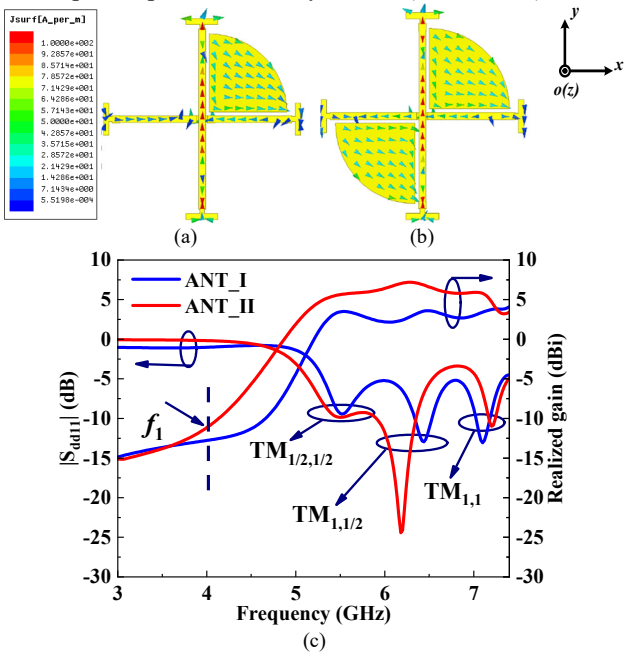

Fig. 2. Surface current distributions at f_1 on (a) ANT_I and (b) ANT_II. (c) Realized gains and $|S_{dd11}|$ of ANT_I and ANT_II.

Case 2: When two patches are placed next to each other to build ANT_III and ANT_IV, two RNs can be introduced. Fig. 4(a) and (c) illustrate their structures and surface current distributions at the frequency of RN_1 which is shown in Fig. 5. As can be seen, strong currents concentrate on the feeding line and very weak currents are on the two patches, thus, the power is reflected to the source, and the radiating of patches are extremely weak to generate RN_1. In Fig. 5, $TM_{1,1}$ mode is moved to a higher frequency, and a distinct weak RN between $TM_{1,1/2}$ and $TM_{1,1}$ is generated at f_2 by the cancelling of the electric field in far field, which attribute to the currents on the patches with an opposite direction although the strong surface currents concentrate on the adjacent patches at f_2, as displayed in Fig. 4(b) and (d). In addition, it can be observed in Fig. 5 that ANT_III has higher realized gain than that of ANT_IV, although the return loss of ANT_III is relatively poor. This is

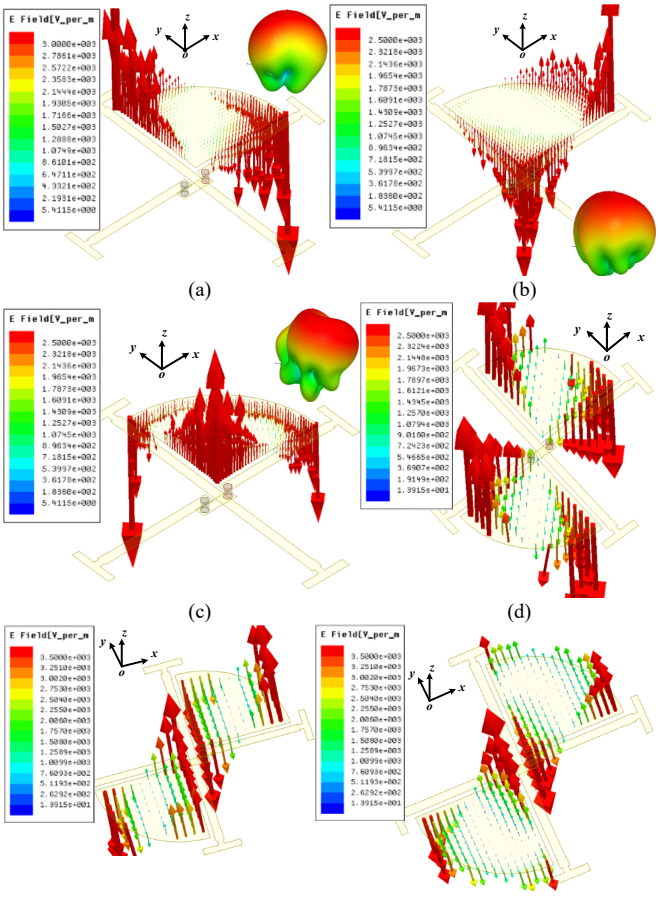

Fig. 3. The v-E-field distributions at (a) $TM_{1/2,1/2}$ of ANT_I, (b) $TM_{1,1/2}$ of ANT_I, (c) $TM_{1,1}$ of ANT_I, (d) $TM_{1/2,1/2}$ of ANT_II, (e) $TM_{1,1/2}$ of ANT_II and (f) $TM_{1,1}$ of ANT_II.

because the differential feeding line of ANT_III almost completely couples to two patches on the right side, while only the upper half of the differential feeding line of ANT_IV couples to two patches. Therefore, ANT_III can couple more energy from the differential feeding line and exhibits higher realized gain compared with ANT_IV.

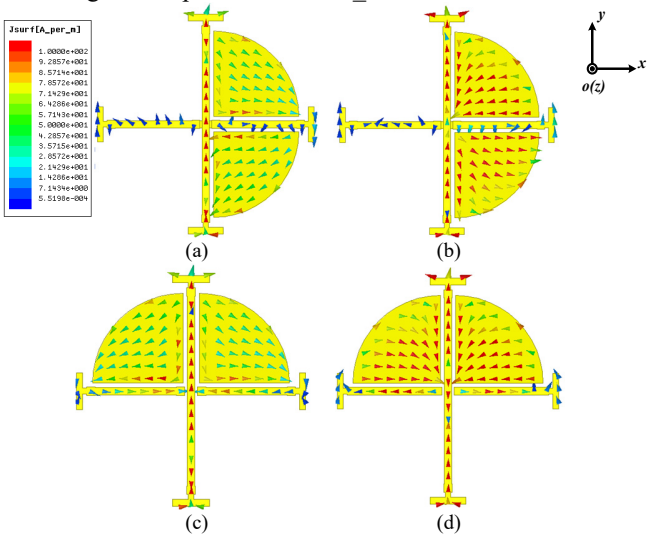

Fig.4. Surface current distributions at (a) RN_1 on ANT_III, (b) f_2 on ANT_III, (c) RN_1 on ANT_IV and (d) f_2 on ANT_IV.

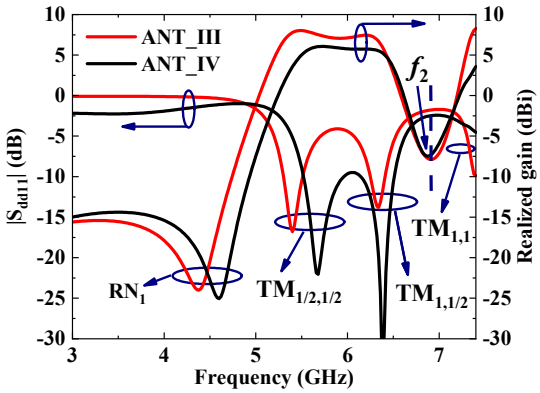

Fig. 5. Realized gains and $|S_{dd11}|$of ANT_III and ANT_IV.

Case 3: Based on ANT_IV, when another patch is placed at the lower left corner, the ANT_V is established as shown in Fig. 6(a), and its simulated realized gain is show in Fig.6(c). It has a similar working principle with **Case 2**, which is demonstrated by Fig. 6(a) and (b). For the weak RN situated at f_4, its surface current distribution is displayed in Fig. 6(b), the cancelling of the electric field in far field of patches ensures this RN to be still generated at the higher stopband. In Fig. 6(c), the newly added patch makes RN_1 becomes a weak RN which located at f_3, due to the change of coupling strength [26].

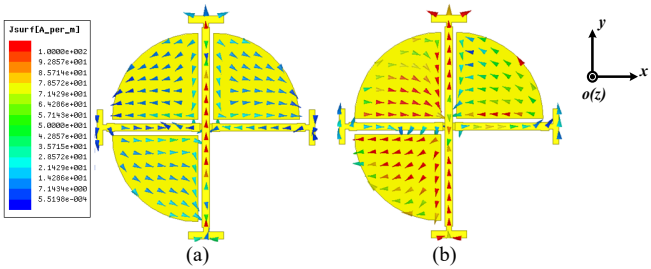

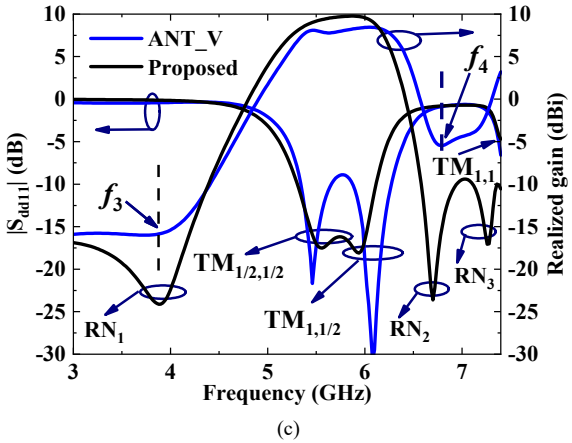

(c)

Fig. 6. Surface current distributions (a) at f_3 on ANT_V, (b) at f_4 on ANT_V. (c) Realized gains and $|S_{dd11}|$of ANT_V and the proposed antenna.

Case 4: When the fourth patch is added, the proposed antenna is established. Its simulated realized gain is depicted in Fig. 6(c). Obviously, the weak RN located at f_4 gets deep to form RN_2 due to further cancellation of the far field electric field. Because of the strong coupling, RN_3 is split out and revealed at the higher stopband. It should be noted that RN_3 is a high-order harmonic null near $TM_{1,1}$. It can be seen that the surface currents at RN_3 also have opposite directions, which is shown in Fig. 7(c), it reveals that RN_3 is also generated by the cancelling of electric field in far field. In addition, when the proposed antenna works, the feeding line operates as coplanar waveguide (CPW) [27], and the quarter patches function as the radiators as well as the finite grounds of the CPW structure [28], [29].

Furthermore, Fig. 7 displays the surface current distributions on the proposed antenna. In Fig. 7(a), (b) and (c), the surface current distributions are consistent with the analysis of **Case 2**, **Case 3** and **Case 4**, respectively. Moreover, the surface current distribution at the center frequency of 5.7 GHz is presented in Fig. 7(d).

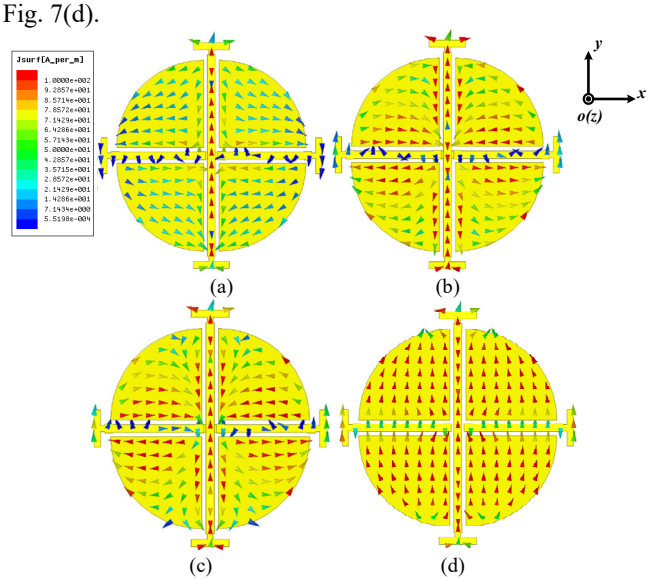

Fig. 7. Surface current distributions of the proposed antenna at the frequency of (a) RN_1, (b) RN_2, (c) RN_3 and (d) 5.7 GHz in the passband.

C. Analysis of The Proposed Filtenna

The coupling scheme of the proposed differential filtenna is given in Fig. 8, where the red nodes denote a pair of differential input, the blue nodes represent the operating modes and the white nodes denote the air (load). Form the coupling diagram, four working paths can be observed: (S+/-)-1-A, (S+/-)-1-2-A, (S+/-)-2-A and (S+/-)-2-1-A. Although the electric field of the quarter circular patch is obtained by symmetrically cutting, the frequencies of desired $TM_{1/2,1/2}$ and $TM_{1,1/2}$ modes can be deduced form the complete circular patch. According to the waveguide cavity model theory [30], the frequencies of $TM_{1/2,1/2}$ and $TM_{1,1/2}$ modes are derived as follows

$$f_{TM_{1/2,1/2}} = f'_{TM_{11}} = \frac{x_{11}c}{2\pi a\sqrt{\varepsilon_r}} \tag{1}$$

$$f_{TM_{1,1/2}} = f'_{TM_{21}} = \frac{x_{21}c}{2\pi a\sqrt{\varepsilon_r}} \tag{2}$$

$$x_{11} = 3.054237, x_{21} = 3.831706 \tag{3}$$

$$a = r\left[1 + \frac{2h}{\pi r\varepsilon_r}\left(\ln\frac{\pi r}{2h} + 1.7726\right)\right]^{1/2} \tag{4}$$

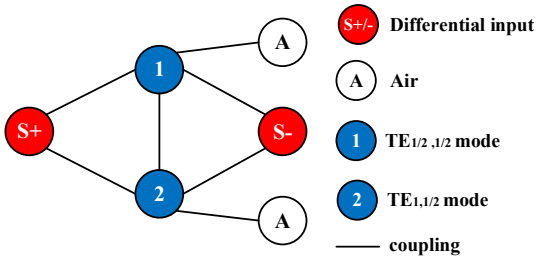

Fig.8. Coupling scheme of the proposed filtenna.

where f represents the resonant frequency of the quarter circular patch, f' represents the resonant frequency of the complete circular patch, c is the light speed in the vacuum, ε_r is the relative permittivity, r denotes the radius of the circular patch and h denotes the thickness of the substrate, respectively. Both the modes of $TM_{1/2,1/2}$ and $TM_{1,1/2}$ can be treated as resonators in the point of view of filter design, so the behavior of the proposed antenna can be analyzed using the filter method. Make $f_1=f_{TM1/2,1/2}$ and $f_2=f_{TM1,1/2}$, the coupling coefficient k_{12} between the two modes can be extracted by

$$k_{12}=\frac{f_2^2-f_1^2}{f_2^2+f_1^2} \tag{5}$$

where f_1 and f_2 are obtained from the S-parameters of two modes with weakly coupled excitation by the external feeding ports, as shown in Fig.9. In addition, the radiation quality factor Q_{rad} of the mode can be evaluated using (6)-(9) [31-32] by analyzing the standalone radiation patches, which is shown in Fig. 9.

$$Q_{rad1}=\frac{f_1}{f_{02}-f_{01}}(1+k) \quad (TM_{1/2,1/2}) \tag{6a}$$

$$Q_{rad2}=\frac{f_2}{f_{04}-f_{03}}(1+k) \quad (TM_{1,1/2}) \tag{6b}$$

$$k=\frac{1-10^{S_{dd11\min}}}{1+10^{S_{dd11\min}}} \quad \text{(resonator is under-coupled)} \tag{7a}$$

$$k=\frac{1+10^{S_{dd11\min}}}{1-10^{S_{dd11\min}}} \quad \text{(resonator is over-coupled)} \tag{7b}$$

$$S^{\phi}_{dd11}=\sqrt{\frac{1+|S_{dd11\min}|^2}{2}} \tag{8}$$

$$S_{dd11}=0.5\cdot(S_{11}-S_{12}-S_{21}-S_{22}) \tag{9}$$

where f_{01}, f_{02}, f_{03} and f_{04} represent four frequencies with $|S_{dd11}|=S^{\phi}_{dd11}$ and $S_{dd11\min}$ is the minimum reflection coefficient at the resonant frequency of f_1 or f_2. To acquire the desired response, the external quality factor Q_{ext} needs to be designed to match Q_{rad}, where a trade-off between Q_{rad1} and Q_{rad2} should be considered. Q_{ext} of our design can be extracted using (10) [33], which can be adjusted by tuning the width W_1 of feeding line and coupling gap S.

$$Q_{ext}=\frac{2\pi f_0\cdot\tau}{4} \tag{10}$$

where τ denotes the group delay of S_{11} at the center frequency of f_0. In this design, the desired filtering response is obtained under the conditions of K_{12}=0.185, Q_{rad1}=31.11, Q_{rad2}=62.54 and Q_{ext}=43.8.

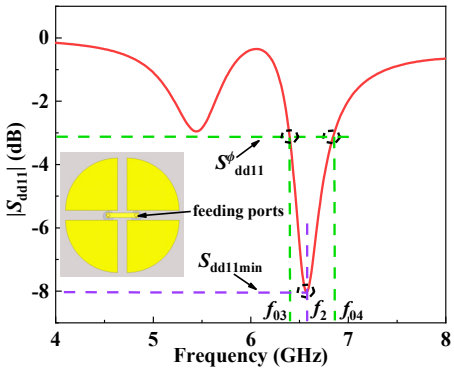

Fig. 9. Calculation procedure for radiation factor Q_{rad} of the proposed antenna.

To establish the equivalent lumped circuit, the electric field (E-field) and magnetic field (H-field) magnitude distributions at $TM_{1/2,1/2}$ and $TM_{1,1/2}$ modes are given in Fig. 10(a)-(d). It can be observed that although the strength of the E-field is much greater than that of the H-field, it indicates that the E-field and the H-field coexist and interact between the feeding line and the patches as well as between adjacent patches. Moreover, as shown in Fig. 1, the differential input and the symmetrical configuration is utilized, a virtual electric wall can be established in the central plane along the x direction according to odd- and even-mode theories [34]. The proposed configuration can be divided into two identical parts along the virtual electric wall when build equivalent lumped circuit. Thus, the equivalent lumped circuit of the proposed filtenna is established as Fig. 11 shown [34-35]. The two radiation patches in the upper or lower half can be considered as a whole, which can be molded by an RLC circuit in parallel, thus, $TM_{1/2,1/2}$ and $TM_{1,1/2}$ modes are further equivalent to a parallel circuit of $C_4L_4R_1$ and $C_5L_5R_2$, respectively. As mentioned above, the E-field and the H-field coexist between the feeding line and the patches as well as between adjacent patches. Therefore, the electromagnetic (EM) coupling between the feeding line and the two patches in the upper or lower half is molded as L_1C_1 in parallel. The EM coupling between a patch and its horizontally adjacent patch is equivalent to a parallel circuit of L_2C_2. Although the virtual electrical wall is built in the central plane along the x axial direction, the upper and lower adjacent patches can still be coupled to each other, so the EM coupling between a patch and its vertically adjacent patch is molded by a parallel circuit of L_3C_3. In addition, the coupling gaps between patches and feeding lines are modeled as a J (admittance) inverter. The results of the equivalent lumped circuit simulated by Advanced Design System 2016 version (ADS 2016) are depicted in Fig. 12, which three nulls are obtained, and good frequency selectivity and stopband rejection are achieved.

The S-parameters of differential ports can be calculated as follows [36]

$$S_{dd11}=0.5\times(S_{11}-S_{12}-S_{21}+S_{22}) \tag{11}$$

$$S_{dd12}=0.5\times(S_{13}-S_{14}-S_{23}+S_{24}) \tag{12}$$

$$S_{dd21}=0.5\times(S_{31}-S_{41}-S_{32}+S_{42}) \tag{13}$$

$$S_{dd22}=0.5\times(S_{33}-S_{34}-S_{43}+S_{44}) \tag{14}$$

where S_{ij} (i, j = 1, 2, 3, 4) represent the S-parameters of the ordinary 4-port network. Fig. 13 displays the effects of the ports location L_0 and the width of coupling gaps S on $|S_{dd11}|$, respectively. It can be observed in Fig. 13(a) that two resonant nodes shift toward each other with the increase of L_0. In Fig. 13(b), frequency of the second resonant node shifts downward along with the decrease of S. Thus, based on above analysis, the bandwidth can be adjusted by changing position of the two resonant nodes.

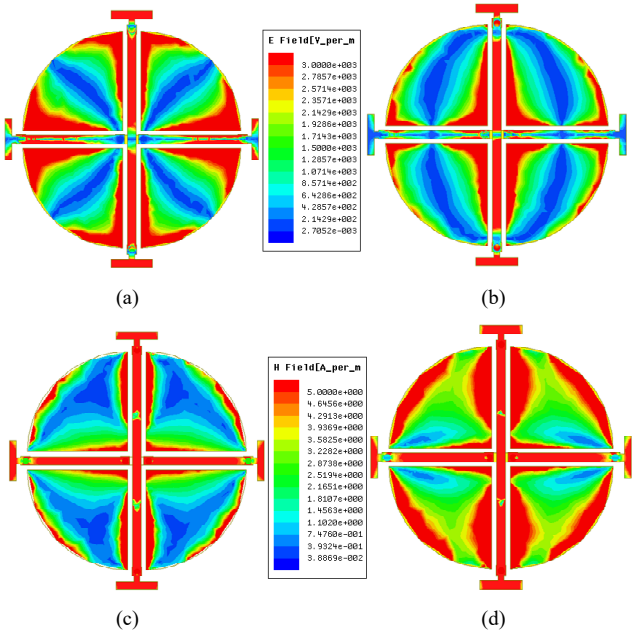

Fig.10. E-field magnitude distributions at (a) $TM_{1/2,1/2}$, and (b) $TM_{1,1/2}$. H-field magnitude distributions at (c) $TM_{1/2,1/2}$, and (d) $TM_{1,1/2}$.

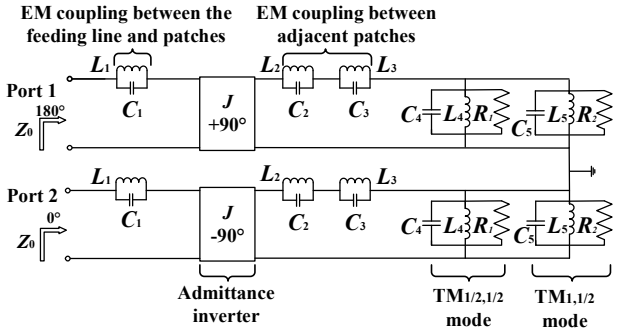

Fig. 11. Equivalent lumped circuit of the proposed antenna (C_1=10.0 pF, C_2=3.8 pF, C_3=6.48 pF, C_4=1.39 pF, C_5=1.06 pF, L_1=0.049 nH, L_2=0.32 nH, L_3=0.095 nH, L_4=0.37 nH, L_5=2.6 nH, R_1=256.6 Ohm, R_2=224.2 Ohm, J=28.59 mS).

Moreover, impacts of some key parameters on the stopband performance are displayed in Fig. 14. As we can see in Fig. 14(a), RN_2 and RN_3 can be controlled by adjusting h_2 with little effects on RN_1, and the stopband rejection in the frequency range from RN_2 to RN_3 can be improved effectively. In Fig. 14(b), R mainly dominates the frequency of RN_2 and adjust the out-of-band rejection in the high frequency. For RN_1, it can be greatly affected by the number of patch and the position of patches, which has been proved in Fig. 5 and Fig. 6(c).

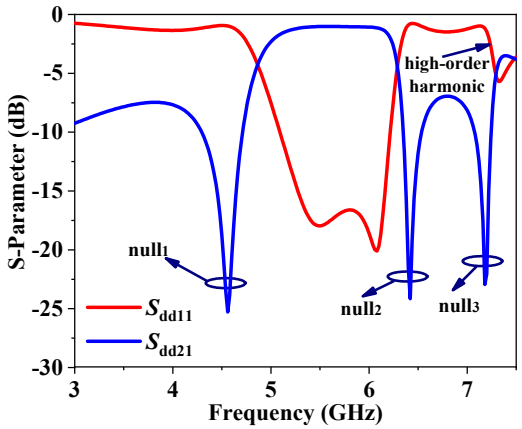

Fig. 12. Simulated results of the equivalent lumped circuit.

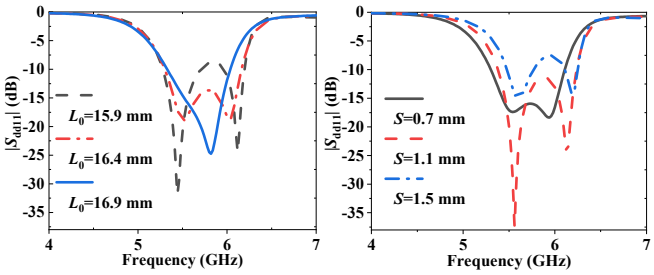

Fig. 13. Effect of (a) ports location and (b) width of coupling gap on $|S_{dd11}|$.

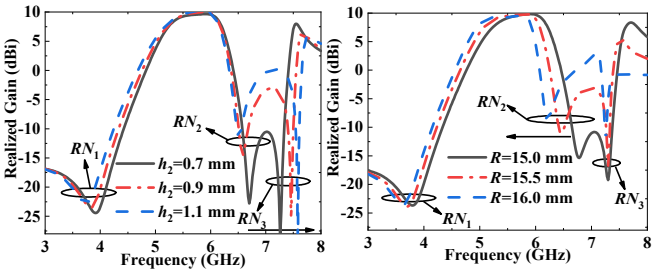

Fig. 14. Effect of (a) thickness of air layer and (b) radius of patches on stopband performance.

III. Simulated and Measured Results

For demonstration, a prototype antenna is simulated, fabricated and measured. The simulated and measured realized gain and S-parameter are illustrated in Fig. 15. The working frequency band ranges from 5.28 to 6.11 GHz and the FBW reaches 14.6%. The measured average gain in the passband is about 9.1 dBi, in which the maximum and minimum measured gain are 9.58 and 8.30 dBi, separately. Three RNs with deep out-of-band suppression of 21.5, 25 and 20 dB, are located at 3.84, 6.7 and 7.36 GHz, respectively. Hence, passband skirt selectivity and out-of-band rejection are improved greatly. Compared with the realized gain in the passband, the stopband rejection level is more than 19 dB. Moreover, the polarization isolation is shown in Fig. 17(a), the simulated and measured polarization isolation are more than 55 dB and 44 dB in the operating band, respectively. Fig. 17(b) shows the efficiency of

Table I. Comparisons between the proposed antenna and reported dual-polarized microstrip patch filtennas

Ref.	DI*	RS* ($\lambda_0\times\lambda_0$)	Profile (λ_0/mm)	FBW*	RNs	Gain (dBi)	Iso* (dB)	CP* (dB)	AE*	SRL* (dB)	FT*	LOS*
[11]	no	0.78×0.78 ↑	0.019/1.63	1.6% ↓	0 ↓	4.9 ↓	>43 ↓	-20 ↓	N.A.	25	open stubs + SIW cavity	2
[15]	no	0.37×0.37	0.069/8 ↑	12.2% ↓	2 ↓	9.4 ↓	>30 ↓	-29	N.A.	40	feeding line + stacked patch	2
[16]	no	0.48×0.48	0.123/10.5 ↑	24.1%	4	8.6 ↓	>30 ↓	-20 ↓	N.A.	30	open stubs + slots + stacked patch	4
[21]	yes	0.8×0.8 ↑	0.06/7 ↑	23%	2 ↓	8.9 ↓	>30 ↓	-22 ↓	N.A.	20 ↓	slots + short pins	1
[22]	yes	0.34×0.34	0.037/3.2 ↑	1.7% ↓	2 ↓	7.5 ↓	>65	N/A	0.84	16 ↓	slots + short pins	1
[23]	yes	0.48×0.48	0.039/0.44	19.5%	4	5.7 ↓	>40 ↓	-44	0.88	27	open stubs + L-probes + square ring	9
[24]	yes	1.08×1.08 ↑	0.185/11.3 ↑	7.6% ↓	2 ↓	8.7 ↓	>37 ↓	N/A	0.85	18 ↓	open stubs + slots	2
[25]	yes	0.2×0.2	0.120/20.03 ↑	4.1% ↓	2 ↓	8 ↓	>-30 ↓	-18 ↓	0.87	15 ↓	stacked patches	4
Prop.	**yes**	**0.63×0.63**	**0.054/2.832**	**14.6%**	**3**	**9.58**	**>44**	**<-29**	**0.87**	**25**	**feeding line + patches (planar)**	**1**

DI* represents differential input; RS* is radiator size; FBW* denotes fractional bandwidth; Iso* is isolation; CP* represents cross-polarization; AE* denotes antenna efficiency; SRL* denotes stopband rejection level; FT* represents filtering technology; LOS* denotes the layer of substrate.

the proposed antenna, where the high radiation efficiency about 87% can be observed. Fig. 16 is the photo of the fabricated prototype. The antenna radiation patterns of vertical polarization at 5.7 and 6.0 GHz are illustrated in Fig. 18, and the low cross-polarization level less than -29 dB is realized. In addition, the measured front-to-back ratios are larger than 18 dB. The measured results agree well with simulated ones.

The comparisons between the proposed antenna and some reported dual-polarized microstrip patch filtennas are listed in Table I. Although reference [11] features the low-profile, the gain and bandwidth need to be further improved, and there is no differential input. In [15], [16] and [25], these designs exhibit the relatively small size and good filtering performance. However, they suffer the high profile, and the multi-layer substrates are used. In [21] and [22], by using slots, short pins and one substrate, the good filtering response is obtained. However, the relatively large size and high profile of 7 mm can be observed in [21], and the narrow band only of 1.7% FBW in [22] requires to be promoted. Although [23] has the properties of small size, low-profile, wideband and four RNs, a total of nine layer substrates are used, and the cost and processing complexity are increased greatly. Furthermore, it can be found that all references utilize multiple types of additional filtering structures, such as slots, short pins, open stubs and stacked patches, etc. As can be seen, only using the feeding line, quarter circular radiation patches and one substrate, our proposed antenna with compact structure not only features the characteristics of differential dual-polarized input and excellent filtering response with three RNs, but also exhibits high gain of 9.58 dBi, FBW of 14.6%, low cross-polarization level less than -29 dB, high isolation more than 44 dB, deep stopband rejection of 25 dB and low profile of 2.832 mm, satisfying the requirements of vehicular communications.

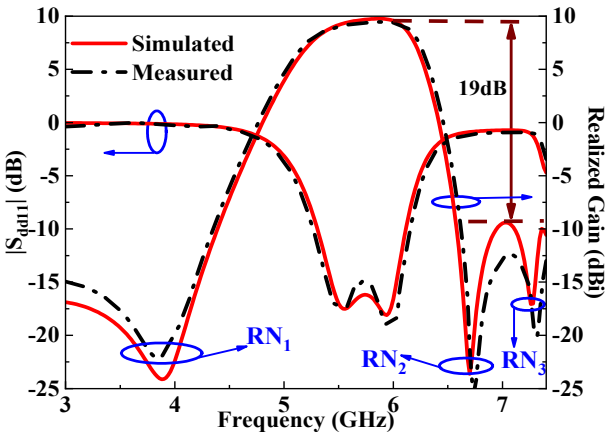

Fig. 15. Simulated and measured results of vertical polarization.

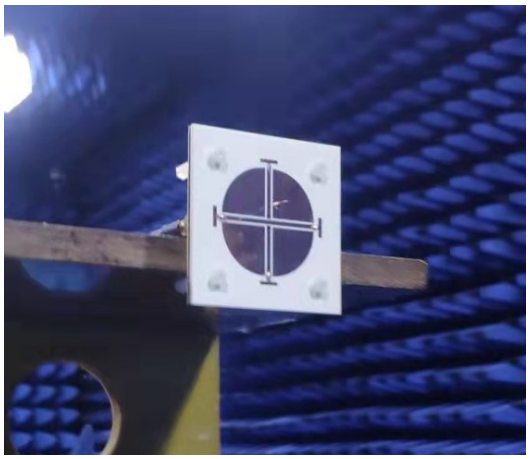

Fig. 16. Photo of the fabricated antenna.

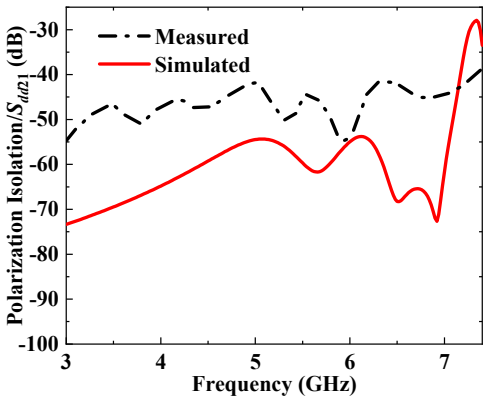

(a)

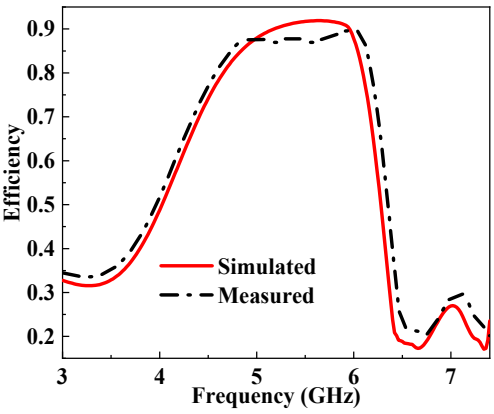

(b)

Fig. 17. (a) Simulated and measured polarization isolation. (b) Simulated and measured efficiency.

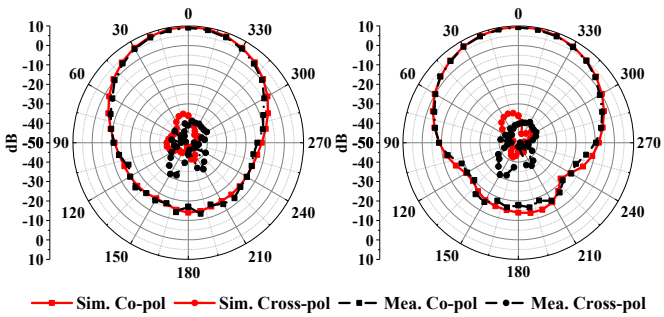

(a) (b)

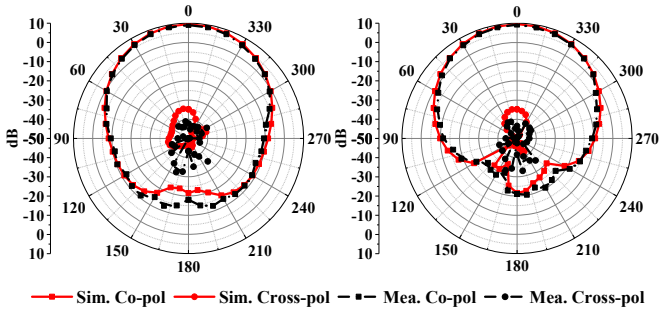

(c) (d)

Fig. 18. Radiation patterns of vertical polarization. 5.7 GHz at (a) E plane and (b) H plane, 6.0 GHz at (c)E plane and (d) H plane.

IV. Conclusions

In this paper, a compact low-profile differential dual-polarized filtenna without an external filter circuit for vehicular communications was proposed. Without utilizing slots, short pins, parasitic/stacked elements, L-shaped probes, open stubs and extra filtering circuits, only by symmetrically and orthogonally embedding a pair of crossed feeding lines into four identical quarter circular patches printed on one substrate, a compact, low-profile, simple and symmetrical configuration is achieved. Three RNs can be generated by the self-structure of the proposed antenna, realizing the great filtering performance with deep out-of-band suppression. The prototype antenna with the FBW of 14.6%, average gain of about 9.1 dBi and the profile only of 2.832 mm was analyzed, fabricated and measured. The measured results agreed well with the simulated ones. Moreover, the measured isolation was more than 44 dB in the passband and the cross-polarization level was less than -29 dB. The excellent performance showed that the proposed antenna is a good candidate for in-vehicle WLAN, in-vehicle Wi-Fi 6E, V2V communication and 5G vehicle-to-basestation communication applications.

References

[1] J. -H. Ou, Z. Chen, S. F. Bo, Y. Zhang and X. Y. Zhang, "Compact Dual-Polarized Antenna with Low-Pass Response for Marine Communication," *IEEE Transactions on Vehicular Technology*, vol. 70, no. 3, pp. 2649-2656, March 2021.

[2] P. Mei, Y. -M. Zhang and S. Zhang, "Decoupling of a Wideband Dual-Polarized Large-Scale Antenna Array With Dielectric Stubs," *IEEE Transactions on Vehicular Technology*, vol. 70, no. 8, pp. 7363-7374, Aug. 2021.

[3] A. Khoshniat, T. Yekan, R. Baktur and K. F. Warnick, "Active Integrated Antenna Supporting Linear and Circular Polarizations," *IEEE Transactions on Components, Packaging and Manufacturing Technology*, vol. 7, no. 2, pp. 238-245, Feb. 2017.

[4] T. L. Foreman, "An antenna coupling model for cross-polarized antennas for radar electromagnetic compatibility analysis," *IEEE Transactions on Electromagnetic Compatibility*, vol. 35, no. 1, pp. 28-35, Feb. 1993.

[5] N. Lambrecht, H. Pues, D. De Zutter and D. V. Ginste, "Modeling of Contact Bounce in a Transient Electromagnetic Compatibility Test for the Analysis and Optimization of Nonlinear Devices," *IEEE Transactions on Electromagnetic Compatibility*, vol. 59, no. 2, pp. 541-544, April 2017.

[6] S. S. Agili and T. K. Ishii, "Electromagnetic Compatibility of PSK–OOK Digital Fiber Communications," *IEEE Transactions on Electromagnetic Compatibility*, vol. 56, no. 6, pp. 1322-1325, Dec. 2014.

[7] W. Li, G. Wei, X. Pan, H. Wan and X. Lu, "Electromagnetic Compatibility Prediction Method Under the Multifrequency in-Band Interference Environment," *IEEE Transactions on Electromagnetic Compatibility*, vol. 60, no. 2, pp. 520-528, April 2018.

[8] S. Shahparnia and O. M. Ramahi, "Electromagnetic interference (EMI) reduction from printed circuit boards (PCB) using electromagnetic bandgap structures," *IEEE Transactions on Electromagnetic Compatibility*, vol. 46, no. 4, pp. 580-587, Nov. 2004.

[9] D. Zhang, E. Cheng, H. Wan, X. Zhou and Y. Chen, "Prediction of Electromagnetic Compatibility for Dynamic Datalink of UAV," *IEEE Transactions on Electromagnetic Compatibility*, vol. 61, no. 5, pp. 1474-1482, Oct. 2019.

[10] H. Chu and Y. -X. Guo, "A Filtering Dual-Polarized Antenna Subarray Targeting for Base Stations in Millimeter-Wave 5G Wireless Communications," *IEEE Transactions on Components, Packaging and Manufacturing Technology*, vol. 7, no. 6, pp. 964-973, June 2017.

[11] Meng, C-M, Wang, J, Shi, J. A substrate integrated cavity-fed dual-polarized filtering patch antenna with high isolation. Int J RF Microw Comput Aided Eng. 2019; 29: e21860.

[12] G. Liu, Y. M. Pan and X. Y. Zhang, "Compact Filtering Patch Antenna Arrays for Marine Communications," *IEEE Transactions on Vehicular Technology*, vol. 69, no. 10, pp. 11408-11418, Oct. 2020.

[13] B. Feng, J. Chen, K. L. Chung, L. Wang and Y. Li, "Dual-Polarized Filtering Magneto-Electric Dipole Antenna Arrays With High Radiation-Suppression Index for 5G New Radio n258 Operations," *IEEE Transactions on Antennas and Propagation*, vol. 70, no. 4, pp. 3058-3063, April 2022.

[14] S. J. Yang, Y. M. Pan, L. Shi and X. Y. Zhang, "Millimeter-Wave Dual-Polarized Filtering Antenna for 5G Application," *IEEE Transactions on Antennas and Propagation*, vol. 68, no. 7, pp. 5114-5121, July 2020.

[15] W. Duan, X. Y. Zhang, Y. -M. Pan, J. -X. Xu and Q. Xue, "Dual-Polarized Filtering Antenna With High Selectivity and Low Cross Polarization," *IEEE Transactions on Antennas and Propagation*, vol. 64, no. 10, pp. 4188-4196, Oct. 2016.

[16] W. Chen, Z. Yu, X. He, J. Zhou and W. Hong, "Enhanced-Stopband Dual-Polarized Filtenna without Extra Circuit for Tile Array Applications," *IEEE Transactions on Antennas and Propagation*.

[17] S. J. Yang, Y. F. Cao, Y. M. Pan, Y. Wu, H. Hu and X. Y. Zhang, "Balun-Fed Dual-Polarized Broadband Filtering Antenna Without Extra Filtering Structure," *IEEE Antennas and Wireless Propagation Letters*, vol. 19, no. 4, pp. 656-660, April 2020.

[18] C. Yeh, K. Chen and C. Wang, "Common-Mode Noise Suppression of Differential Serpentine Delay Line Using Timing-Offset Differential Signal," *IEEE Transactions on Electromagnetic Compatibility*, vol. 57, no. 6, pp. 1457-1465, Dec. 2015.

[19] M. Kim, "Periodically Corrugated Reference Planes for Common-Mode Noise Suppression in High-Speed Differential Signals," *IEEE Transactions on Electromagnetic Compatibility*, vol. 58, no. 2, pp. 619-622, April 2016.

[20] C. K. Chin, Q. Xue and H. Wong, "Broadband Patch Antenna With a Folded Plate Pair as a Differential Feeding Scheme," *IEEE Transactions on Antennas and Propagation*, vol. 55, no. 9, pp. 2461-2467, Sept. 2007.

[21] W. Yang, M. Xun, W. Che, W. Feng, Y. Zhang and Q. Xue, "Novel Compact High-Gain Differential-Fed Dual-Polarized Filtering Patch Antenna," *IEEE Transactions on Antennas and Propagation*, vol. 67, no. 12, pp. 7261-7271, Dec. 2019.

[22] Y. I. A. Al-Yasir, Naser Ojaroudi Parchin, Mohammad N. Fares, Ahmed Abdulkhaleq and Maryam Sajedin., "New High-Gain Differential-Fed Dual-Polarized Filtering Microstrip Antenna for 5G Applications," 2020 14*th European Conference on Antennas and Propagation (EuCAP)*, 2020, pp. 1-5.

[23] Y. Zhang, W. Yang, Q. Xue, J. Huang and W. Che, "Broadband Dual-Polarized Differential-Fed Filtering Antenna Array for 5G Millimeter-Wave Applications," *IEEE Transactions on Antennas and Propagation*, vol. 70, no. 3, pp. 1989-1998, March 2022.

[24] Y. Li, Z. Zhao, Z. Tang and Y. Yin, "Differentially Fed, Dual-Band Dual-Polarized Filtering Antenna With High Selectivity for 5G Sub-6 GHz Base Station Applications," *IEEE Transactions on Antennas and Propagation*, vol. 68, no. 4, pp. 3231-3236, April 2020.

[25] J. W. Wang, S. Sun, R. Ma and X. Y. Zhang, "Compact Dual-Polarized Filtenna With Steep Roll-Off Rate for Base Stations," *IEEE Antennas and Wireless Propagation Letters*, vol. 21, no. 8, pp. 1698-1702, Aug. 2022.

[26] Y. Zhang, X. Y. Zhang and Y. Pan, "Compact Single- and Dual-Band Filtering Patch Antenna Arrays Using Novel Feeding Scheme," *IEEE Transactions on Antennas and Propagation*, vol. 65, no. 8, pp. 4057-4066, Aug. 2017.

[27] Terry C. Edwards; Michael B. Steer, "CPW Design Fundamentals," Foundations for Microstrip Circuit Design, IEEE, 2016, pp.384-442.

[28] Y. -J. Lu, Y. -W. Liu and P. Hsu, "A Hybrid Design of Printed Antenna Fed by Coplanar Waveguide With and Without Back Conductor," *IEEE Antennas and Wireless Propagation Letters*, vol. 13, pp. 1597-1600, 2014.

[29] X. Chen, L. Han, X. Chen, Q. Zeng and W. Zhang, "A Wideband Coplanar Waveguide Antenna Array With Series Feed," *IEEE Antennas and Wireless Propagation Letters*, vol. 16, pp. 565-568, 2017.

[30] R. Garg, P. Bhartia, and I. Bahl, *Microstrip Antenna Design Handbook*. Boston, MA, USA: Artech House, 2001.

[31] Y. Yusuf and X. Gong, "A vertical integration of high-Q filters with patch antennas with enhanced bandwidth and high efficiency," 2011 *IEEE MTT-S International Microwave Symposium*, 2011, pp. 1-4.

[32] R. J. Cameron, C. M. Kudsia, and R. R. Mansour, *Microwave Filters for Communication Systems: Fundamentals, Design, and Applications*. Hoboken, NJ, USA: Wiley, 2007.

[33] J.-S. Hong and M. J. Lancaster, *Microstrip Filters for RF/Microwave Applications*. New York, NY, USA: Wiley, 2001.

[34] Liang, J, Huang, G‐L, Zhang, S, Yuan, T, Zhang, G‐M, Amin, M, "Compact differential‐fed dual‐band antenna via loading shorting pin," Int J RF Microw Comput Aided Eng. 2018; 28: e21497.

[35] Daotong LI, Yaqing YU, Ming-Chun Tang, Dajiang LI, Dongmei MU, Mei LI, Active, compact, wideband, receiving filtenna with power adaptation for space-limited wireless platforms, Chinese Journal of Aeronautics, Vol. 35, no. 8, pp. 7-11, 2022.

[36] Y. P. Zhang and Z. Chen, "The Wheeler Method for the Measurement of the Efficiency of Differentially-Driven Microstrip Antennas," *IEEE Transactions on Antennas and Propagation*, vol. 62, no. 6, pp. 3436-3439, June 2014.

ZHIRUI ZHENG received B.S. degree in electric and information engineering, from West China Normal University (CWNU), Nanchong, China, in 2019. Now, he is currently pursuing the Ph.D. degree in information and communication engineering in Chongqing University (CQU), Chongqing, China. His research interests include filtering antennas and filters.

Daotong Li (S'15-M'16) received the Ph.D. degree in electromagnetic field and microwave technology from the University of Electronic Science and Technology of China (UESTC), Chengdu, China, in 2016.

He is currently with the Center of Communication and Tracking Telemetry Command, Chongqing University, Chongqing. Since 2015, he has been a Visiting Researcher with the Department of Electrical and Computer Engineering, University of Illinois at Urbana–Champaign, Urbana, IL, USA, with financial support from the China Scholarship Council. He has authored or coauthored over 60 peer-reviewed journal or conference papers.

His current research interests include RF, microwave and millimeter-wave technology and applications, microwave power transmission (MPT), antennas, devices, circuits and systems, and passive and active (sub-) millimeter-wave imaging and radiometer. Dr. Li was a recipient of the UESTC Outstanding Graduate Awards by the Sichuan province and UESTC in 2016. He was a recipient of the National Graduate Student Scholarship from the Ministry of Education, China, and "Tang Lixin" Scholarship. He is serving as a Reviewer for several IEEE and IET journals, and many international conferences as a TPC Member, a Session Organizer, and the Session Chair.

Xiaoheng Tan received the B.E. and Ph.D. degrees in electrical engineering from Chongqing University, Chongqing, China, in 1998 and 2003, respectively. He was a Visiting Scholar with the University of Queensland, Brisbane, Qld., Australia, from 2008 to 2009. He is currently a professor with the School of Microelectronics and Communication Engineering, Chongqing University. His current research interests include modern communications technologies and systems, communications signal processing, pattern recognition, machine learning, antennas and filters.

Qiang Chen received the B.E. degree from Xidian University, Xi'an, China, in 1986, and the M.E. and D.E. degrees from Tohoku University, Sendai, Japan, in 1991 and 1994, respectively. He is currently the Chair Professor of the Electromagnetic Engineering Laboratory, Department of Communications Engineering, School of Engineering, Tohoku University. His research interests include antennas, microwave and millimeter wave, antenna measurement, and computational electromagnetics. Dr. Chen is a Fellow of the Institute of Electronics, Information and Communication Engineers (IEICE). He received the Best Paper Award and the Zenichi Kiyasu Award in 2009 from the IEICE. He served as the Chair of the IEICE Technical Committee on Photonics-Applied Electromagnetic Measurement from 2012 to 2014, the Chair of the IEICE Technical Committee on Wireless Power Transfer from 2016 to 2018, and the Chair of the Tokyo Chapter of the IEEE Antennas and Propagation Society from 2017 to 2018. He is the Chair of the IEICE Technical Committee on Antennas and Propagation.